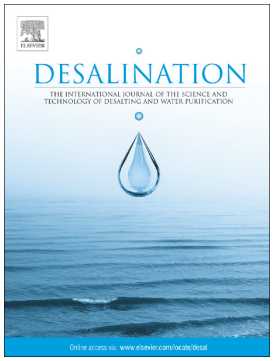

Electro-spun graphene-enriched carbon fibres with high nitrogen-contents for electrochemical water desalination

Yolanda Belaustegui, Saioa Zorita, Francisco Fernández-Carretero, Alberto García-Luis, Fabiola Pantò, Sara Stelitano, Patrizia Frontera, Pierluigi Antonucci, Saveria Santangelo

PII:	S0011-9164(17)31045-7
DOI:	doi:10.1016/j.desal.2017.11.019
Reference:	DES 13512
To appear in:	*Desalination*
Received date:	17 May 2017
Revised date:	24 October 2017
Accepted date:	8 November 2017

Please cite this article as: Yolanda Belaustegui, Saioa Zorita, Francisco Fernández-Carretero, Alberto García-Luis, Fabiola Pantò, Sara Stelitano, Patrizia Frontera, Pierluigi Antonucci, Saveria Santangelo , Electro-spun graphene-enriched carbon fibres with high nitrogen-contents for electrochemical water desalination. The address for the corresponding author was captured as affiliation for all authors. Please check if appropriate. Des(2017), doi:10.1016/j.desal.2017.11.019

Electro-spun graphene-enriched carbon fibres with high nitrogen-contents for electrochemical water desalination

Yolanda Belaustegui[1,#], Saioa Zorita[1], Francisco Fernández-Carretero[1], Alberto García-Luis[1], Fabiola Pantò[2], Sara Stelitano[3], Patrizia Frontera[4,5], Pierluigi Antonucci[4,5], Saveria Santangelo[4,#,*]

[1] *Tecnalia Research & Innovation, Materials for Energy and Environment Area, E-48160 Derio-Bizkaia, Spain*

[2] *Dipartimento di Ingegneria dell'Informazione, delle Infrastrutture e dell'Energia Sostenibile (DIIES), Università "Mediterranea", Reggio Calabria, Italy Università "Mediterranea", DIIES, 89122 Reggio Calabria, Italy*

[3] *Dipartimento di Fisica (DF), Università della Calabria, 87036 Arcavacata di Rende, Italy.*

[4] *Dipartimento di Ingegneria Civile, dell'Energia, dell'Ambiente e dei Materiali (DICEAM), Università "Mediterranea", 89122 Reggio Calabria, Italy*

[5] *Consorzio Interuniversitario per la Scienza e la Tecnologia dei Materiali (INSTM), Firenze, Italy*

Abstract Electro-spun carbon fibres doped with very high nitrogen concentrations (19−21 wt%) are obtained operating carbonisation at low temperature (500°C). The as-synthesised fibres are evaluated as electrode materials for the electrochemical desalination of water. The effect of the enrichment of the nitrogen doped carbon fibres with thermally reduced graphene oxide is also investigated. The fibrous electrodes are able to remove amazing amounts of NaCl (17.0−27.6 mg/g) from a salty solution with an initial concentration of 585 mg/L. The nitrogen doping, which dramatically improves the wettability, plays a crucial role in determining the outstanding electro-sorption capacities of the fibres. It allows fully profiting of the more favourable pore size distribution in the graphene-enriched fibres, endowed with higher conductivity and capacitance, for the obtainment of unprecedented electro-sorption capacities via an extremely simple synthesis process, with no need of activation treatments.

[*] **Corresponding author**
Tel.: +39.0965.1692305. Fax.: +39.0965.1692201. E-mail address: saveria.santangelo@unirc.it (Prof. Saveria Santangelo)
[#] Both authors contributed equally to this study

1. Introduction

The ever-increasing demand of fresh water supply caused by increasing population and environmental contamination has encouraged the water desalination technologies worldwide to move forward in a cost-effective and energy-efficient direction [1]. The capacitive deionization (CDI) method, based on the formation of electrical double layers inside the pores of the electrode material [2,3], is one of the most attractive among them. CDI, also known as electro-sorptive desalination, is an environmentally friendly technology since no secondary contaminant is released during the process. CDI removes salts from water by using two oppositely charged carbon electrodes. On applying a voltage, the surface of the electrodes gets charged and an electrical double layer is formed between the electrode and the solution. These charged electrodes adsorb the counter ions present in the feed water on their pores and thereby, desalinate it. Once these pores are saturated with salt ions, the cell voltage is reduced, reversed or shorted to regenerate the electrodes and the previously stored ions are released into a waste water solution. The greatest advantage of CDI is its high theoretical energy efficiency for desalination [4]. For instance, the intrinsic energy required by CDI for brackish waters is ≈0.1 kWh m^{-3} [4], which is inferior to that of reverse osmosis (≈0.2 kWh m^{-3}), the most efficient technique presently available [1,4,5]. Another noteworthy advantage is its low equipment and operational costs because CDI is a low-pressure, non-membrane based desalination process that is controlled by a low applied voltage (0.8–1.2 V) and can be of great help in remote areas.

The CDI performance depends intimately on the physical and structural properties of the electrode materials. High specific surface area, high conductivity, and appropriate pore size distribution are basic electrode requirements [2,3]. In this scenery, carbon materials represent the ideal candidates as the CDI electrodes. Various nanocarbons, such as carbon nanotubes, carbon aerogel, mesoporous carbon, and activated carbon, have been successfully utilised to fabricate the electrodes in CDI cells [2,3,6].

Synthesising hybrid carbon nanostructures with tailored physical/chemical properties may represent the route to obtain engineered electrode materials with advanced electrochemical performances. A viable strategy contemplates the use of suitable additives. Thanks to its superior electronic conductivity and mechanical properties, graphene represents the ideal conductive additive for the fabrication of hybrid nanostructured electrodes [7]. Indeed, in spite of its worse performances, graphene oxide (GO) is routinely used in place of graphene [7,8] because of its better dispersibility in solvents, low-cost and large-scale production enabled by the chemical exfoliation method.

Several studies have demonstrated that doping carbon-based materials is a successful alternative strategy to tailor their physical/chemical properties [3,6,9−17]. It has been shown that the introduction of defects, heteroatoms and/or functional groups at the carbon surface can increase available active sites and enhance the reactivity and conductivity [12,14]. In particular, due to the presence of additional lone pairs of electrons, nitrogen atoms can provide carries for the electronic conduction [6,9,18]. Actually, nitrogen-doped nanocarbons exhibit improved electro-catalytic and electro-chemical properties [3,6,10−17]. Moreover, nitrogen doping has been recently shown to increase the wettability of the electrode materials by the electrolyte, resulting in the pseudocapacitive effect [3,6,16−18].

Specifically, in the field of CDI, from the porous electrode theory [2] it is well known that also intra-particle macro- and micro-pores of the electrode have influence over the effective concentration of the adsorbed salt. Electro-spinning (ES) is a very simple, scalable and inexpensive technique for the growth of one-dimensional nanostructures featured by hierarchical porosity (intertwined micro-, meso-, and macro-pores) [19−22]. Since the preparation of CDI electrode materials via ES occurs in two well distinct steps (namely, fibrous film deposition and thermal treatment of the as-spun film) there is the possibility of *continuously* depositing (over rotating drums) electro-spun

fibres that will be thermally treated subsequently. This feature, together with its scalability, makes ES the most suitable technique for the large-scale production of CDI electrodes.

This contribution deals with synthesis, analysis and testing, as electrode materials in CDI cells, of electro-spun nitrogen-doped carbon fibres (N-CFs) and graphene-enriched nitrogen-doped carbon fibres (G/N-CFs), as obtained via thermal reduction of GO during the post-spinning fibre carbonisation step.

Nitrogen-doping of the electro-spun fibres can be very easily obtained by the use of a nitrogen-containing polymer, such as polyacrylonitrile, $(C_3H_3N)_n$, featured by 26.4 wt% N-content, as a component of the spinnable solution. Previous studies have demonstrated that the nitrogen content of the heat-treated fibres decreases with increasing carbonisation temperature [22]. This is because, during the polymer carbonisation, cross-linking condensation reactions between two monomer units of the adjacent ladder polymeric molecular chains occur in the 300−500°C temperature range, causing evolution of water vapour, whereas if the temperature further rises, also volatile nitrogen-containing by-products (such as hydrogen cyanide, HCN, and ammonia, NH_3) are expelled from the fibres [23]. Therefore, in order to obtain fibres with high nitrogen-doping levels, in the present study, carbonisation temperature was set at 500°C, the lowest value ever reported at the best of the authors' knowledge.

Dufficy et al. [15] have recently reported on the synthesis of composite anodes for lithium-ion battery consisting of carbon nanofibres containing thermally reduced graphene oxide. The fibres were prepared via ES followed by heat treatment at 650°C, by dispersing in the spinnable solution different GO loads (1−20 wt%, relative to the polymer concentration), with 5 wt% GO load giving the best electrochemical performances. Based on these results, G/N-CFs were here prepared by the addition of 5 wt% GO to the spinnable solution. It has been proposed that removal of oxygen functional groups of GO occurs at temperatures as low as 200°C, producing a defective C sp^2 structure able to improve the electrical conductivity of the host amorphous matrix [15]. Thus, the incorporation of GO into the carbon fibres is expected to generate beneficial effects on their properties in spite of the low carbonisation temperature selected (500°C). The performance of the produced materials was tested in the desalination of sodium chloride solutions by using CDI technology.

2. Experimental

2.1. Sample preparation

Table 1 reports the composition of the spinnable solution utilised for the preparation of the N-CFs and the G/N-CFs. Polyacrylonitrile (PAN, purity: 99.9%, average molecular weight: 150000 g/mol) and *N*,*N*-dimethylformamide (DMF, purity: 99.8%) acted as polymer and solvent, respectively. PAN and DMF were supplied by Sigma-Aldrich and were used without further purification. Graphene oxide (GO) was obtained from graphite powder (Sigma-Aldrich; lateral size: < 20 μm) via a modified Hummers method [24]. In brief, $K_2S_2O_8$ (3 g) and P_2O_5 (3 g) were added to a suspension of graphite powder (2 g) in concentrated H_2SO_4 (40 mL) for pre-oxidation. After suspension heating, the solid, recovered by centrifugation, was repeatedly washed with water and dried. Subsequently, pre-oxidized graphite was added to concentrated H_2SO_4 (90 mL) and stirred in an ice bath. $NaNO_3$ (2 g) and $KMnO_4$ (12 g) were then added under vigorous stirring, keeping temperature within 10°C. The solution obtained was kept for 5 days at room temperature (RT). After water (250 mL) addition, the suspension was heated and 30 wt% H_2O_2 (20 mL) was added. Finally, after filtering and washing with 2 M HCl solution (300 mL), the suspension was repeatedly washed with water and dried. Further details can be found elsewhere [25]. The obtainment of GO was ascertained by carrying out micro-Raman spectroscopy (MRS) and x-ray diffraction (XRD) analyses (Fig. S1). The O/C atomic ratio, as determined by x-ray photoelectron spectroscopy (XPS) was 0.55.

Table 1. Sample codes, composition of the spinnable solutions, results of the morphological analysis by SEM, and information about specific surface area (SSA), specific micro-pore volume (SMPV) and adsorption average pore size (d_P) The fibre diameter range, as automatically calculated by the image analysis software, is reported; d_F stands for the value at which the diameter distribution is centred.

Sample code	Composition of the spinnable solution			SEM analysis results		SSA (m^2/g)	SMPV (mm^3/g)	d_P (nm)
	PAN (wt%)	DMF (wt%)	GO (wt%)	*d* range (nm)	d_F (nm)			
N-CFs	6.50	93.50	0.00	135–1180	360	20.32	2.57	4.37
G/N-CFs	6.50	93.17	0.33	110–1070	340	16.76	1.29	4.62

The PAN/DMF solution for the synthesis of the N-CFs was prepared by dissolving polymer in the solvent and magnetically stirring until a clear and homogenous solution was obtained. In order to synthesise the G/N-CFs, GO was ground to finer powders and dispersed in the solvent (no chemical functionalisation was necessary [26]). The GO suspension was sonicated for GO further exfoliation purposes. Finally, PAN was incorporated in the suspension, and the as-obtained solution was magnetically stirred for 4 h. The GO relative amount of the solution (0.33 wt%, corresponding to a concentration of 5 wt% relative to the polymer) was chosen on the basis of the results on graphene-containing carbon nanofibres for lithium-ion battery anodes recently reported by Dufficy et al. [15].

The as-prepared PAN/DMF and GO/PAN/DMF solutions were electro-spun using a CH-01 Electro-spinner 2.0 (Linari Engineering s.r.l.). The apparatus (Fig. S2a) consists of a syringe equipped with a stainless steel needle, a grounded aluminium collector, and a high voltage power supply. During the spinning process, the collector is continuously translated along direction perpendicular to the syringe axis. The spinnable solution, fed at a constant rate by means of a pump that moves the syringe piston, is ejected under the high voltage applied between the syringe nozzle and the collector. For further technical details on the spinning set-up, see ref. [21]. In the present case, a 20 mL syringe, equipped with a 40 mm long 0.8 mm gauge stainless steel needle, was utilised. Solution was fed at a volumetric rate of 1.41 mL/h. A 15 kV voltage over an 11 cm collection distance was applied. The spinning process was carried out in an open-air environment (relative air humidity: 40%) at 20±1°C temperature.

DMF very rapidly evaporates during the ES owing to strong jet elongation [27]. At the end of the process, the obtained non-woven fibrous PAN and GO/PAN membranes (outsets of Fig. S2a) were peeled from the collector and thermally processed. First, an oxidative treatment was performed, on each membrane, in order to stabilise the polymer. PAN is thermally stable up to 322°C [22]. Upon oxidation at a temperature lower than 322°C, chemical reactions (such as cyclisation, dehydrogenation, cross-linking) occur, through which PAN is converted to an infusible stable ladder polymer [23]. This treatment (stabilisation) enables its subsequent processing at temperature higher than 322°C to obtain graphite-like structures (carbonisation) [23]. The latter step is operated under vacuum or inert atmosphere [23,28]. In the present case, PAN and PAN/GO fibres were stabilised for 3 h in static air at 280°C, as usual [28], and subsequently carbonised for 3 h upon 100 cm^3/min helium flow. Both the thermal treatments were operated increasing temperature at a rate of 5°C/min, and were followed by uncontrolled cooling down to RT. Carbonisation was carried out at a relatively low temperature (500°C). It is known that nitrogen doping of the carbon fibres has positive effects on the electrochemical performance of carbon-based battery anodes, in terms of lithium-ion storage [29]. Previous studies demonstrated that the nitrogen content of the fibres decreases with increasing carbonisation temperature [22]. This is because evolution of water vapour occurs during PAN carbonisation at temperatures in the 300−500°C range, whereas above 500°C also volatile nitrogen-containing by-

products (such as HCN and NH_3) are expelled from the fibres. Therefore, in order to obtain fibres with high nitrogen-doping levels, carbonisation temperature was set at 500°C. Note that the choice of a low temperature further reduces energy consumption, thus making cheaper the electrode material production process. Paper-like self-supporting membranes were obtained at the end of the thermal processing (inset of Fig. S2b). The PAN-based membrane was mechanically robust and bendable, as previously obtained under similar conditions [22]. Conversely, the GO/PAN-based one was fragile and broke under bending.

Often, in order to improve wettability and/or to form porous structure, carbonaceous materials are activated by means of harsh chemical oxidants such as KOH [12] or piranha-solution [30] before their use as CDI electrodes. No activation was carried out on the present samples before their electrochemical testing.

2.2. Sample characterisation

Texture and morphology of the thermally processed samples were investigated by scanning electron microscopy (SEM). A Phenom Pro-X scanning electron microscope equipped with an energy-dispersive x-ray (EDX) spectrometer was utilised for SEM analysis. Fibermetric software allowed for automated accurate fibre diameter measurements from their SEM images.

The specific surface area of the carbonaceous mats was determined via the Brunauer-Emmmett-Teller (BET) method. Quantification of the gas amount adsorbed to form a monolayer on the solid surface was carried out by using ASAP 2010 Micromeritics equipment. Before measurements, the samples were degassed at 150ºC in a vacuum ($50{\cdot}10^{-3}$ mm Hg) for 8 h in order to remove superficial impurities. N_2 adsorption-desorption isotherms were recorded in multiple equilibrium steps until the saturation of the sample at N_2 liquid cryogenic temperature (−196°C). From them, the porous structure characteristics of the membranes were also inferred. As usual [31], following the Barrett-Joyner-Halenda (BJH) approach the pore size distribution was obtained and the *t*-plot method was utilised to calculate the the specific micro-pore volume. The average adsorption pore size was also estimated. The results obtained are reported in Table 1.

Raman scattering was measured in air at RT using a confocal set-up and a NT-MDT NTEGRA - Spectra SPM spectrometer. The system was equipped with MS3504i 350 mm monochromator and ANDOR Idus CCD. A solid-state laser operating at 2.33 eV provided excitation; two suitable RazorEdge Filters prevented Rayleigh-scattered laser light from reaching the detection system. A Mitutoyo high numerical aperture 100X objective collected the scattered light from the sample. The use of a very low laser power (250 μW at the sample surface) prevented local heating of the samples and annealing effects. Spectra were analysed by using a commercially available spectroscopic analysis software package.

XRD patterns were recorded with a Bruker D2 Phaser diffractometer equipped with a Ni β-filtered Cu-K_α radiation (λ=0.1541 nm). Further details on the instrumentation utilised can be found elsewhere [22].

Surface composition of the samples and chemical environment of the component species were investigated by XPS. The spectra were acquired using a Surface Sciences Instruments M-Probe, equipped with a monochromatic Al-K_α source (1486.6 eV). As usual [11], the binding energy shifts were calibrated keeping the C 1*s* position fixed at 284.5 eV. Gauss–Lorentzian shaped bands were used to fit measured spectral profiles. The elemental concentrations were estimated from the areas under the photoelectron peaks weighed by the relative sensitivity factors. Identification and quantification of the surface species were carried out by decomposing the high-resolution photoelectron spectra of core levels.

2.3. Working electrode preparation and electrochemical three-cell measurements

2.3.1. Preparation of the N-CFs and G/N-CFs electrodes

N-CFs and G/N-CFs electrodes were prepared by mixing as-carbonised materials, polyvinylalcohol (PVA, Tecnalia) added as a binder and ethanol as solvent following the procedure schematically depicted in Fig. S3a. The mixture was stirred for at least 8 h until obtaining the slurry. The slurry was cast onto a graphite sheet (Graftech International), which acted as current collector and dried in a 60°C oven overnight to remove the organic solvents and to form an N-CFs and G/N-CFs sheet. The composition of the prepared electrodes was 90wt% of as-carbonised materials and 10wt% of PVA.

For the electrochemical measurements the size of the electrodes was 2.5 cm^2. For the CDI experiments N-CFs and G/N-CFs electrodes were cut into square pieces of 9 cm^2 surface area. These electrodes were assembled into capacitive deionization device for testing.

Prior to their use in the electro-sorption experiments, a conditioning protocol was performed to the electrodes. This protocol consisted in immersing all the electrodes in 0.1M NaCl solution, for at least 24h, to wet the pores of the electrodes [32]. Then, the electrodes were placed in the CDI cell passing deionization water in order to remove the possible ions physically adsorbed. At this point, we began the electro-sorption experiments with the target NaCl solution.

2.3.2. Electrochemical measurements

The electrochemical performance of the electrodes and the electrical double layer formation were evaluated by cyclic voltammetry (CV) and electrochemical impedance spectroscopy (EIS). CV measurements were done with a conventional three electrode system using a computer controlled potentiostat/galvanostat (AUTOLAB PGSTAT302N, Metrohm) at RT (Fig. S3a). The working electrode was prepared using the as-carbonised mats (2.5 cm^2 area), the counter electrode was graphite and the reference electrode was a standard Ag/AgCl electrode.

CVs were performed with sweep rates of 5–100 mV/s in the potential range from −1 to 0.5V in 0.1mol/L NaCl solution. The values for specific capacitance of the CDI electrode material were calculated from the current-voltage curves according to the following equation:

$$Cs = \frac{1}{vm}\int \frac{I}{V}\, dV \qquad (1)$$

where C_s (F/g) is the specific capacitance, I (A) is the response current, V (V) is the potential, v (V/s) is the potential scan rate and m (g) is the mass of the electro-active materials in the electrodes.

EIS analysis was conducted to determinate the internal resistance of the electrodes. The measurements were performed with AUTOLAB PGSTAT302N using the three compartment cell. The amplitude of the alternating voltage was 0.01V around the equilibrium potential (0 V) and the data were collected in the frequency range from 10000Hz to 0.1Hz.

2.4. Electro-sorption experiments of CDI

To investigate the electro-sorptive capacity of the N-CFs and G/N-CFs electrodes, batch mode experiments were carried out in a continuously recirculating system including a symmetric electro-sorptive unit cell, two reservoirs, a peristaltic pump (Fisher Scientific, Mini-pump variable flow), a conductivity meter (Hanna Microprocessor Conductivity/TDS meter) and an external power supply (DC Lab Power supply LABPS1503). CDI unit cell consisted of two parallel fibre-based electrode sheets of 9 cm^2 area separated by a non-electrically conductive spacer. This prevented electrical short circuit and allowed water to flow along the electrodes. In each experiment, a solution of NaCl was employed as the target solution with a total volume of 100 mL. The flow rate was 7.7mL/min and the applied voltage 1.2 V. During the experiment, the solution temperature was kept at 25°C, and the conductivity was continuously monitored and converted to the sodium chloride concentration. This was

accomplished by using the linear relationship between salt concentration, [NaCl] (mg/L), and conductivity of the solution, σ (μS/cm),

[NaCl] = 0.6708 σ – 341.94, (2)

obtained via the calibration procedure carried, prior to the experiment, in the range of initial conductivity of NaCl solutions between 1382 and 17950 μS/cm, which corresponded to the concentrations of 585 and 11700 mg/L, respectively.

In order to calculate the salt adsorption capacity *SAC* (mg/g) of the CDI electrodes, i.e. the amount of adsorbed salt ions per unit weight of the electrode, it was applied a fixed cell voltage and maintained until the cell charging was complete and salt concentration was constant through the cell [33]. As usual [6], the salt adsorption capacity was calculated via the equation:

$$SAC = Q = \frac{(C_0 - C_t)\, v}{m} \quad (3)$$

where, C_0 (mg/L) is the initial concentration, C_t (mg/L) is the instantaneous concentration at time t (min) in equilibrium, v (L) is the solution volume and m (g) is the total mass of the two (active) electrodes.

3. Results and discussion

3.1. Sample properties

Figures 1a,b and S2b,c show the morphology of the samples, as resulting from SEM analysis. The sample obtained by heat treatment of the as-spun PAN fibres is featured by greater spatial homogeneity than that obtained from carbonisation of the GO/PAN fibres (compare Figs.S2b and c). The morphology of the latter sample, with thermally reduced graphene oxide (TRGO) sheets dispersed throughout the mat (Fig. 1b), is in line with

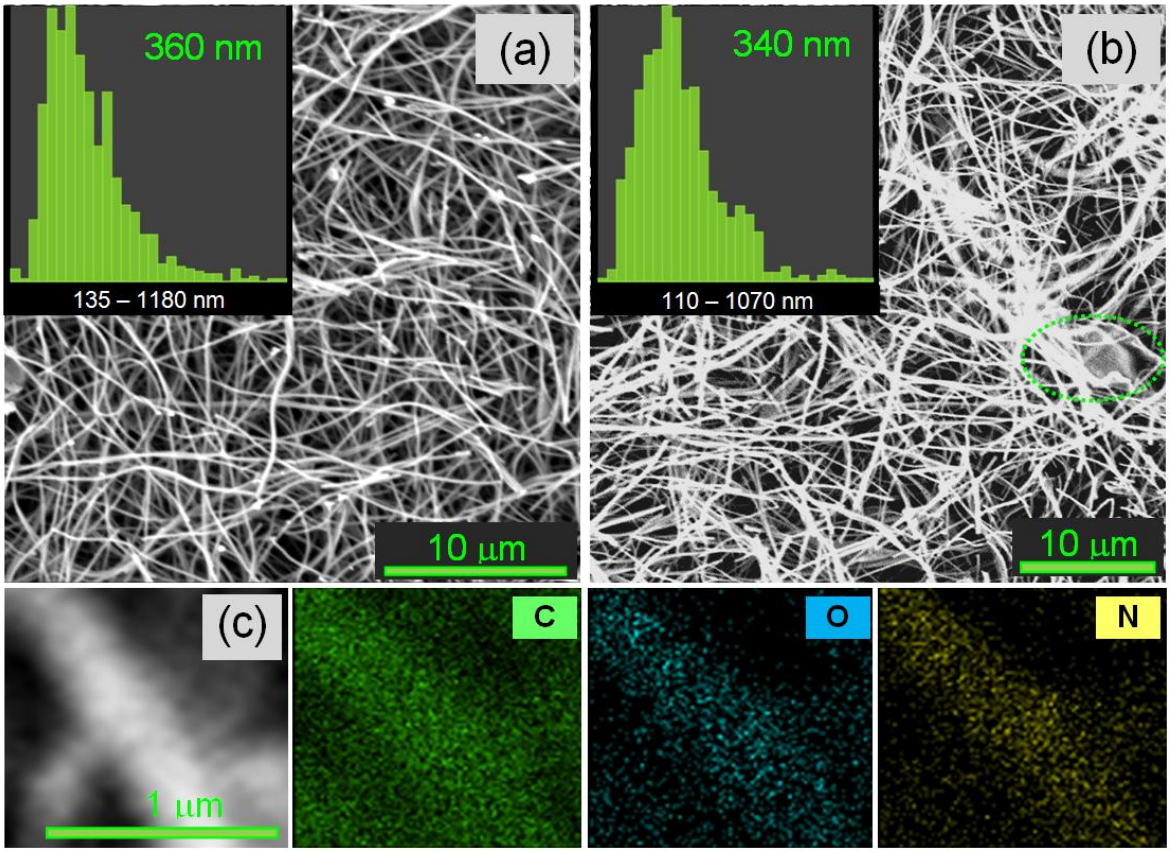

Fig. 1 (a,b) Morphology and (c) elemental composition of the samples, as resulting from SEM analysis. SEM images refer to (a) N-CFs and (b) G/N-CFs. Insets: fibre diameter distribution with peak value and diameter range, as automatically calculated by the image analysis software. The shown elemental maps refer to G/N-CFs.

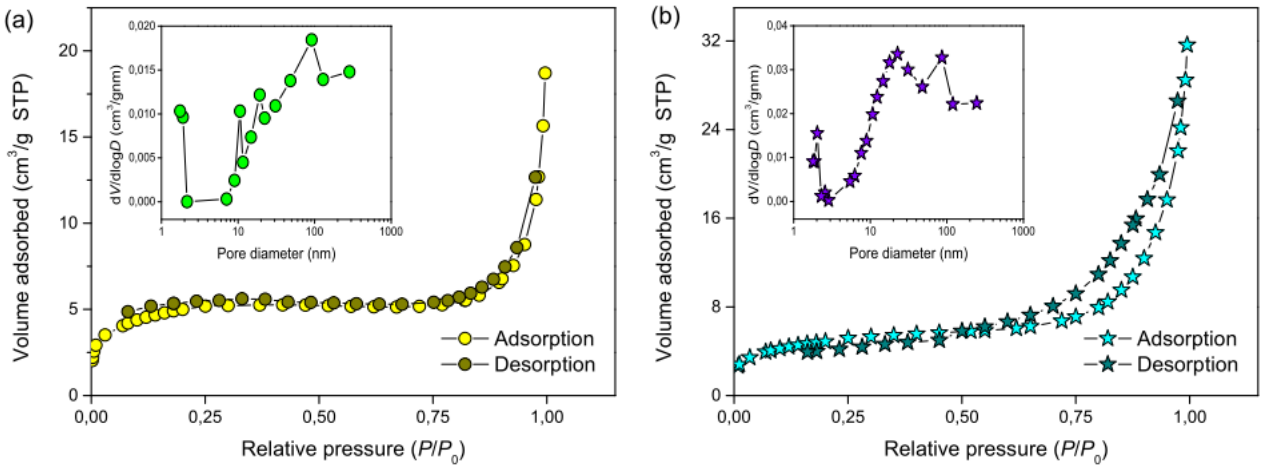

Fig. 2. Nitrogen sorption isotherms and pore size distributions (insets) of (a) N-CFs and (b) G/N-CFs.

expectations [15]. In this case, the fibres are shorter, which explains the reduced mechanical robustness of the membrane, and slightly thinner than in the other sample (Table 1). The smaller diameter of the fibres is understood as an effect of the GO polarity [8,22], whereas the shorter length might be due to the jet fragmentation induced by the exfoliation of GO sheets owing to the high shear in the ES process [15].

Table 1 reports the specific surface area (SSA), specific micro-pore volume (SMPV), and average pore size (d_P) of N-FCs and G/N-CFs electrode materials. The low carbonisation temperature here selected is responsible for the moderate SSA values obtained [13,18]. The N_2 adsorption/desorption isotherms and pore size distributions are shown in Figs. 2a and b and related insets. The N-CFs show an isotherm of type I according to BDDT classification [34], which indicates the presence of micropores. In the case of G/N-CFs, the isotherm exhibits a typical type IV behaviour and the presence of steep slope at higher relative pressures (>0.5), which points out mesoporosity and macroporosity [35]. Although N-CFs exhibit larger SSA and SMPV with respect to G/N-CFs (Table 1), by comparing the pore size distributions of the two samples (insets of Figs. 2a and b) it comes out that the G/N-CFs comprise a large fraction of mesopores (2−50 nm) and macropores (>50nm), which is believed to be an optimal situation for electro-sorption in CDI process [2,3]. Besides, mesopores in G/N-CFs have an average diameter of 4−5 nm, which is suitable for access by ions.

The results of EDX analysis (Fig. 1c) prove that the samples are nitrogen-doped. Residual oxygen is also present, associated to compounds inherent to stabilised PAN [15]. The dispersion of carbon, oxygen and nitrogen within the fibres is spatially uniform, as evidenced by the elemental mapping.

The surface composition of the samples was determined by analysing the survey XPS profiles (Fig. 3). The results (Table 2) confirmed the high-level of nitrogen doping of the fibres. The values of the atomic concentration inferred from the quantitative analysis of the photoelectron spectra were 18.7 and 17.5 at% for N-CFs and G/N-CFs, respectively. These values, fully consistent with those previously obtained at 600°C carbonisation temperature [22], correspond to nitrogen relative weights (19.3−20.8 wt%), by far higher than those previously reported for nitrogen-doped nanocarbons [9,10,12,14]. For instance, carbon nanofibre webs obtained from polypyrrole carbonisation and KOH activation [12] and N-doped graphene obtained by the exposure of graphene to

nitrogen plasma [10] contained 10.2 and 9.5 wt% nitrogen, respectively. Comparable nitrogen amounts (9.6 wt%) were obtained for porous carbon derived from zeolitic imidazolate frameworks [3]. Nitrogen contents up to 8.4% were reported for nitrogen-doped carbon nanotubes prepared using melamine precursor [9], whereas only 4.7 at% N was present in porous nitrogen-doped carbon nanosheets prepared via simultaneous activation and graphitization of biomass-derived natural silk [14]. In protic salt derived porous carbons, N content decreased from 12.5 to 2.5 at% with carbonisation temperature increasing from 700 to 1000°C [18]. The greater N-doping level of the C fibres produced by electro-spinning is due to the use, as a component of the initial solution, of a polymer (PAN) featured by a high (26.4 wt%) N-content combined to the choice of a low carbonisation temperature that limits the release of volatile N-containing by-products [22,23], with beneficial effects on the safety and the environmental friendliness of the fibre production process.

Table 2. Results of the quantitative analysis of the XPS, HRXPS and MRS spectra.

Sample codes	XPS analysis			HRXPS analysis			MRS analysis	
	C (at%)	N (at%)	O (O/C) (at%)	pyridinic-N (at%)	pyrrolic-N (at%)	graphitic-N (at%)	I_D/I_G	L_C (nm)
N-CFs	74.5	18.6	6.9 (0.09)	9.6	6.5	2.5	2.54	1.73
G/N-CFs	73.5	17.5	9.0 (0.12)	9.0	6.1	2.4	2.49	1.77

The investigation of high-resolution XPS (HRXPS) spectra of C 1*s* core level (Fig. S4) confirmed the presence of C−N bonds at 285.3 eV [14]. Information on the nature of the nitrogen species at the surface of the N-CFs and G/N-CFs and their relative amounts was deduced from the analysis of HRXPS spectra of N 1*s* core level (inset of Fig. 3). Nitrogen functional groups generally observed in nitrogen-doped nanocarbons include pyridinic-, pyrrolic- and quaternary nitrogen at 398.5, 400.4 and 401.4 eV binding energy (BE), respectively [9−14,22,36]. N-oxides of pyridinic-N at 402−405 eV BE may be also present [3,10,11,13,36].

Each of pyridinic-N atoms, located at the edge of graphene planes (Fig. S5), replaces a C atom in the hexagonal C-ring and donates one *p*-electron to the aromatic π system; pyrrolic-N atoms are bonded to two C atoms (C−N=C) in the pentagonal C-rings and contribute to the π system with two *p*-electrons; quaternary-N atoms, also known as ‘‘graphitic-N’’ or ‘‘substituted-N’’ atoms, replace C atoms within a graphene layer, bonding with three C atoms [3,9,10,36]. Finally, bonding of N-oxides of pyridinic-N (N^+–O^-) is with two C atoms and one O atom. It is well assessed that nitrogen doping enhances the pseudo-capacitance, improves the conductivity and increases the electrode's surface wettability through hydrophilic functional groups [3,6,16−18]. Conversely, the role played by these species in determining the electrochemical behaviour of the nanocarbons is still controversial. For instance, pyridine-type nitrogen is known to have positive effects on the storage of lithium ions [8,29], whereas pyrrolic- and graphitic-N seem to be more important for the electro-catalytic activity of N-doped nanocarbons [10,11].

By investigating HRXPS spectra of N 1*s* core level, it is found that pyridinic-N, pyrrolic-N, and graphitic-N are present on the surface of N-CFs and G/N-CFs. In both the samples, pyridine-type nitrogen is the most abundant species (~51%), followed by the pyrrolic one (~34%). The absence of N-oxides of pyridinic-N is consistent with the selected oxidation temperature [13].

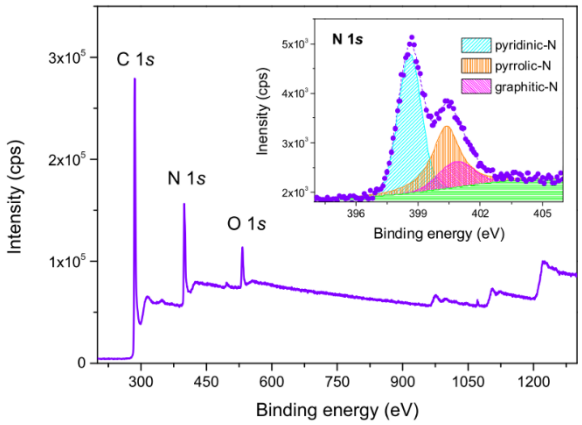

Fig. 3. Survey XPS spectrum measured in G/N-CFs. Inset: surface species contributing to the HRXPS spectrum of N 1*s* core level.

According to Wang et al [37] the graphitic mole fraction (x_G) obtainable by carbonisation of the PAN fibres depends on the absolute temperature (T) at which the heat treatment is carried out, namely $x_G = 0.691exp(-7360/RT)$, with R denoting the ideal gas constant, and is generally quite low (e.g. $x_G = 0.37$ for a carbonisation temperature of 1200°C). For T = 500°C (present case), this empirical relationship gives a x_G-value of 0.22. The low graphitisation degree and the high level of nitrogen doping of the fibres are responsible for the detection of a very intense "disorder" band in the Raman spectra of both the samples (Fig. 4). As well-known [9,10,11,14,38,39], the D-band (at 1346 cm^{-1}, for 2.33 eV excitation) arises from the breathing mode of C hexagonal rings and is activated by the presence of (bond-angle, bond-length, hybridisation) disorder and heteroatoms in the graphitic carbon network. Conversely, the G-band (at 1582 cm^{-1}), associated to the stretching of all C=C pairs, is the fingerprint of the graphitic crystalline arrangement. Therefore, the higher the amorphousness degree and the doping level of the material are, the higher the D/G intensity ratio (I_D/I_G) is [10,11,14,39].

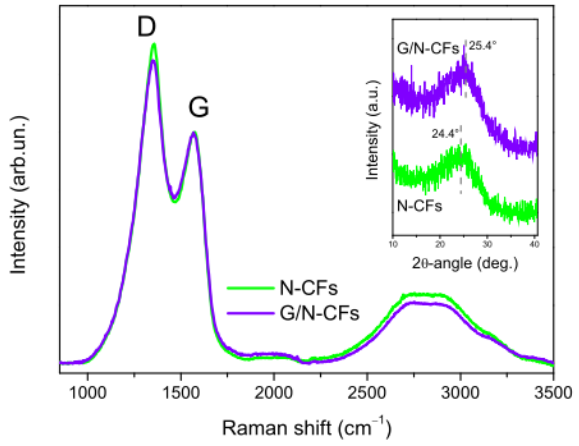

Fig. 4 Raman spectra of the samples. The spectra are normalised to the G-band maximum intensity for an easier comparison. Inset: XRD patterns.

In the G/N-CFs I_D/I_G slightly lowers with respect to N-CFs (Table 2). Although very small, this change is in agreement with literature reports [15]. Together with the lower intensity in the second order mode region, it is indicative of the beneficial effects (in terms of average crystallinity) of the presence of TRGO sheets dispersed throughout the mat (Fig. S6). In fact, having a less defective structure than the PAN-derived fibres carbonised at 500°C, TRGO causes the composite mat to be, on the whole, more ordered [15]. Actually, on one hand, the average size (L_C) of domains with graphitic order, estimated from I_D/I_G ratio via Tuinstra-Koening relationship [40],

$L_C = 4.4/I_D/I_G$, increases from 1.7 nm in N-CFs to 1.8 nm in G/N-CFs. On the other hand, in G/N-CFs the very broad (002) peak associated to the amorphous/disordered carbon lattice [15] shifts towards higher 2θ-angles (inset of Fig. 4), confirming the higher average graphitisation degree of the TRGO-containing fibres [3,41].

Very interestingly, in both the samples, the G-band is detected at around 1564 cm^{-1}. The remarkable downshift of its frequency position can be regarded as a further proof of the nitrogen-doping [9], since it can be ascribed to the electron transfer from the dopant nitrogen atoms to the π-states in carbon matrix (see also Fig. S6).

3.2. Electrochemical performance

CV curves of N-CFs and G/N-CFs electrodes were measured in a potential window of -1 – 0.5 V at different scan rates (5, 10, 20, 30, 40, 50 and 100 mV/s) in 0.1 M NaCl solutions to ascertain the electrical double-layer (EDL) formation. For fixed scan rate, no marked difference is observed comparing the CV curves of the two electrode materials investigated. The curves (Figs. 5a and b) of both the electrodes show deviation from the ideal rectangular shape of the double-layer capacitor. These deviations, slightly more evident in the case of N-CFs (compare anodic regions of the curves), indicate the occurrence of Faraidac pseudo-capacitive reactions [42]. They are associated to the presence of nitrogen functional groups incorporated in an appreciable amount [16]. In fact, a similar behaviour has been reported also for N-doped graphene [16]. However, in graphene containing 7 at% of nitrogen, the deviations from double-layer behaviour become evident only at high scan rates [16]. Differently, in the present case, owing to the larger concentration of N atoms (17.5−18.6 at%), the effect of Faraidac pseudo-capacitive reactions on the shape of CV curves is visible at any scan rate. The CV curves clearly demonstrate that N/G-CFs possess superior capacitive performance compared to N-CFs, indicating that they should have a better electro-sorption performance than N-CFs, as actually N-doped graphene does with respect to graphene [16].

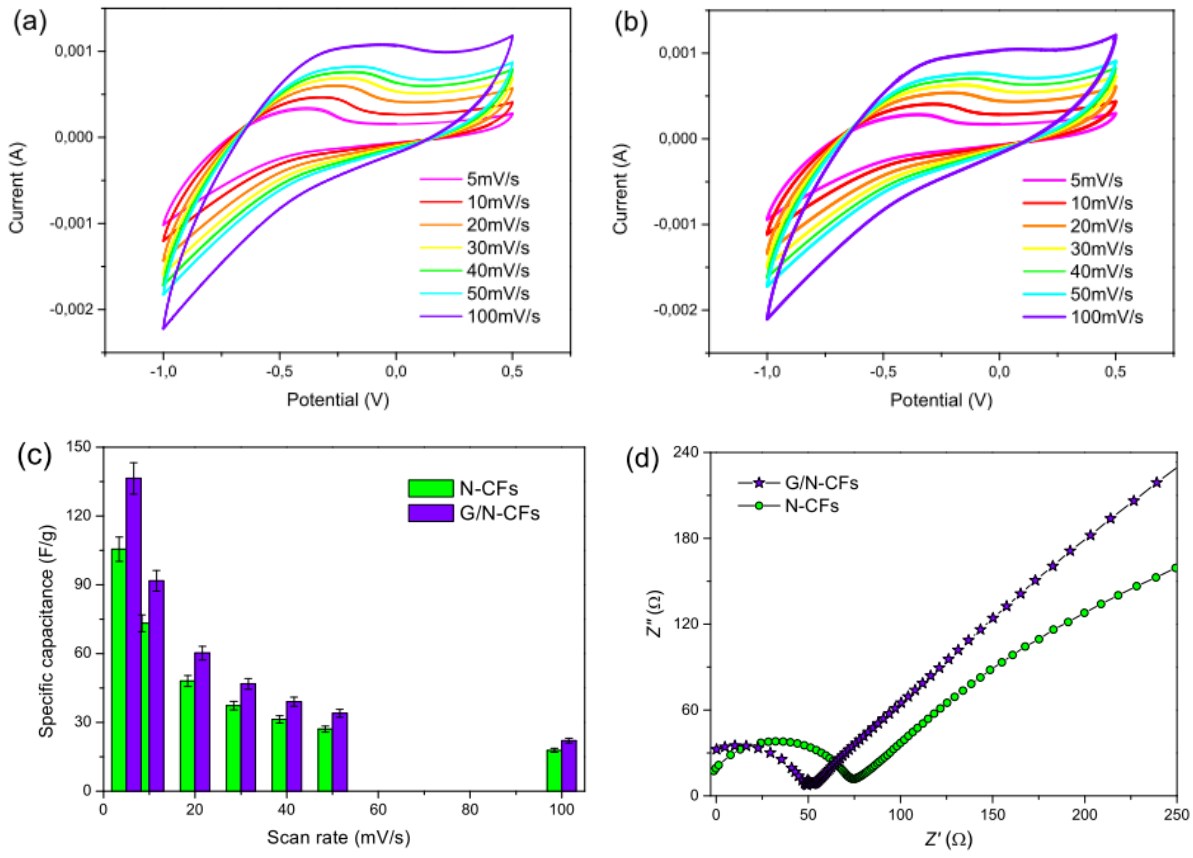

Fig. 5. Electrochemical properties of the N-CFs and G/N-CFs. (a,b) CV curves of (a) N-CFs and (b) G/N-CFs measured in a potential window of -1 – 0.5 V at different scan rates, (c) specific capacitance as a function of scan rate, and (d) Nyquist plots obtained from EIS analysis.

Figure 5c compares the specific capacitance of N-CFs and G/N-CFs, calculated from CV curves via eq.(1), at different scan rates. At any scan rate, higher C_S values pertain to the G/N-CFs. For instance, at 5 mV/s, the specific capacitance of G/N-CFs (136.38 F/g) is ~30% larger than that of N-CFs (105.50 F/g). The greater C_S values obtained for G/N-CFs prove that the incorporation of graphene in the nitrogen doped carbon electrode improves its conduction properties and, as a consequence, its specific capacitance, implying that G/N-CFs have a greater potential in CDI application with respect to N-CFs [16]. C_S values measured for N-CFs and G/N-CFs are very close to those reported for nanoporous carbon prepared respectively from mono- (Zn) and bi-metallic (Zn,Co) zeolitic methylimidazolate framework [3], by heat treatments at much higher temperatures (900°C). In both the electrodes, C_S values remarkably decrease (from 105.50 down to 17.84 F/g for N-CFs, and from 136.38 down to 22.02 F/g for G/N-CFs) with increasing scan rate (from 5 to 100 mV/s), in agreement with the literature [3]. At low scanning rates, the ions of the electrolyte have enough time to diffuse into the inner pores of the electrodes, which is essential for the formation of the EDL, therefore, more ions are adsorbed on the surface of the electrodes. As the scan rate increases, time is not enough for the ions to move and accumulate into the inner pores and, as a result, the accessible area would be lower and the formation of EDL would be incomplete.

The electrochemical behaviour of the N-CFs and G/N-CFs electrodes was evaluated also by EIS analysis, recognised as one of the principal methods to examine the inner resistivity of a carbon electrode [42]. Figure 5d displays the Nyquist plots of the electrodes at 0.1 M NaCl concentration. The plots exhibit similar shapes, consisting of two contributions. The straight spike line (with comparable slopes of ~45°) at the low frequency region represents the Warburg impedance, which depends on the kinetics of the ion diffusion in solution, as well as, on the adsorption of ions onto the electrode surface [19]. The small quasi-semicircle at the high-frequency region corresponds to a parallel combination of the charge-transfer resistance and the double-layer capacitance [6], as resulting from the contact between the electrode and current collector and the resistance of the porous electrode itself [19]. The size of this semicircle, which increases as the barrier for ions' entry to the pores enhances [43], is smaller in the case of G/N-CFs, indicating that graphene introduction in carbon fibres should be beneficial to the charge transfer on electrode. The electrolyte accessibility becomes easier for the larger pores, while the ions do not easily enter the smallest pores. Thus, lower resistance is associated with better electrolyte pore accessibility [19].

3.3. Desalination performance of the fabricated electrodes

CDI performance of the fabricated electrodes was measured in a symmetric batch-mode CDI pilot plant doing continuous recycling of water. The volume of NaCl solution was 100 mL; the initial concentrations varied between 11700 and 585 mg/L, since, as known [6], if the total dissolved solid is higher than 500 mg/L, water is not suitable for drinking. The cell voltage and the flow rate were 1.2 V and 7.7 mL/min, respectively. A pair of squared electrodes, 3 cm x 3 cm in size, was used. The total mass of the electrode pair was accurately measured to subsequently calculate the salt adsorption capacity of the CDI electrodes. The measured mass values ranged between 50 and 80 mg. To check the reproducibility, several experiments were carried out on each type of electrode material (N-CFs or G/N-CFs), and the corresponding SAC was calculated averaging over the values obtained in these experiments. In order to evaluate the electro-sorption capacity of the electrodes at different initial concentrations of NaCl solutions, the concentration change of the NaCl was measured by a conductivity meter at the outlet of the cell, where the solution was released. When the potential is applied, Na^+ and Cl^- are attracted onto the surface of the oppositely charged electrodes, causing the conductivity of the NaCl solution to decrease, as shown in Fig. 6. A dramatic decrease in the conductivity occurs in the early stage of the process, when the concentration of the saline solution in the CDI cell undergoes a noticeable change, indicating quick adsorption of

the salts ions. Conversely, in the subsequent stage, the conductivity varies more slowly until the adsorption equilibrium is reached due to the electro-sorption saturation [42]. Figure 6 compares the desalination performance of the G/N-CFs and N-CFs electrodes in 585 mg/L and 11700 mg/L NaCl solutions (Figs. 6a and b, respectively). It is evident that the desalination performance of the electrodes containing graphene is higher than that of N-CFs electrodes. No bubble formation or pH change was observed during experiments.

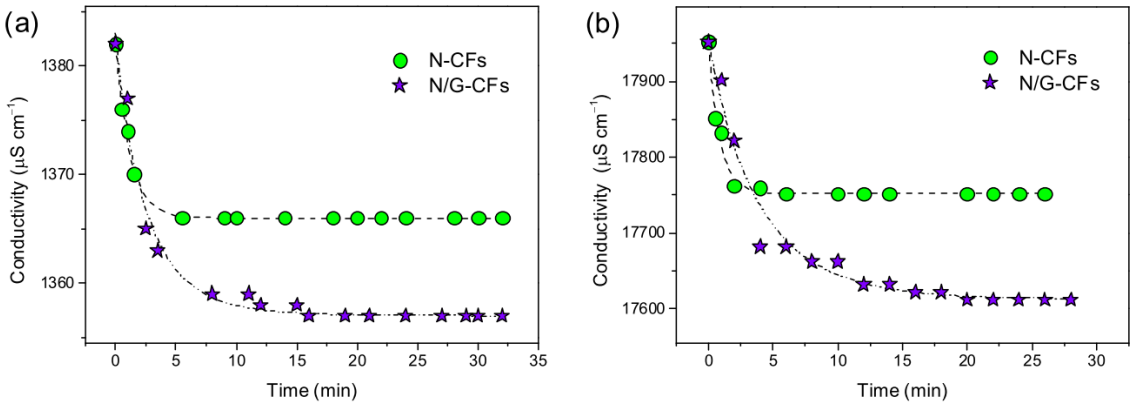

Fig. 6. Desalination performance of N-CFs and G/N-CFs electrodes with (a) 585 mg/L NaCl and (b) 11700 mg/L NaCl solutions.

The numerical electro-sorption capacity of the electrodes was calculated via eq. (3). The concentration of NaCl was determined by converting the measured conductivity values via eq. (2). Figure 7 compares the electro-sorption capacity of the N-CFs and G/N-CFs electrodes at various concentrations. As a general trend, under constant voltage, the electro-sorption capacity gradually increases with increasing NaCl concentration revealing that the concentration has a positive impact on electro-sorption performance of the electrodes. Moreover, with the concentration increasing from 585 mg/L to 11700 mg/L, the electro-sorptive capacity is gradually enhanced from 19.96 mg/g to 211.94 mg/g for N-CFs electrodes and from 27.55 mg/g to 360.30 mg/g for G/N-CFs electrodes. This is due to the enhanced mass transfer rate of ions inside the pores and reduced EDL overlapping effects, since double-layer thickness is inversely proportional to the solution concentration [30,42,44]. The incorporation of graphene in the synthesis of G/N-CFs led to a higher electro-sorption capacity of the G/N-CFs electrodes at the all concentrations. In fact, it causes the conductivity of the NaCl solution to reduce to larger extent with respect to the N-CFs electrode, which means that more ions were adsorbed in its pores. Developing specific surface area is generally desired for CDI desalination [45], however, as pointed out also by Xu et al [16], SSA is not the only or the most influential factor. In fact, although N-doped graphene has a relatively low SSA, it exhibits the highest electro-sorption capacity among graphene-based electrodes in similar experimental conditions [16]. With few exceptions there is no linear relationship between the specific surface area and capacity, mainly because the SSA is commonly measured by small N_2 molecules. The small pores, which can be accessed by N_2, may constrain the accessibility of ions in the NaCl solution. In our case, specific surface area seems to have little effect on the capacity of the electrodes, thus electro-sorption capacity ought to be significantly affected by other factors. That is, the mechanism that determines the electro-sorptive performance is complicated and other factors including pore microstructure, pore size distribution and surface groups can play important roles on this value [46]. Figure 7 shows the electro-sorption capacity of G/N-CFs is higher than of N-CFs in all the cases although its SSA value was lower, in agreement with literature [16]. In the case of G/N-CFs has large ion capacity due to the complex structure, which is built by carbon nanofibres doped with nitrogen and graphene. Most of the pores in the G/N-CFs electrode are of the type of mesopores and macropores according to the SEM and BET results. These mesopores exhibit very

complicated structure and tortuous tunnels, which allow fast transport of the ions to the adsorption sites [47]. On the other hand, the electro-sorption of both the nitrogen-doped fibres is by far greater (Fig. S7) than that reported for other carbon based hybrids [18,30].

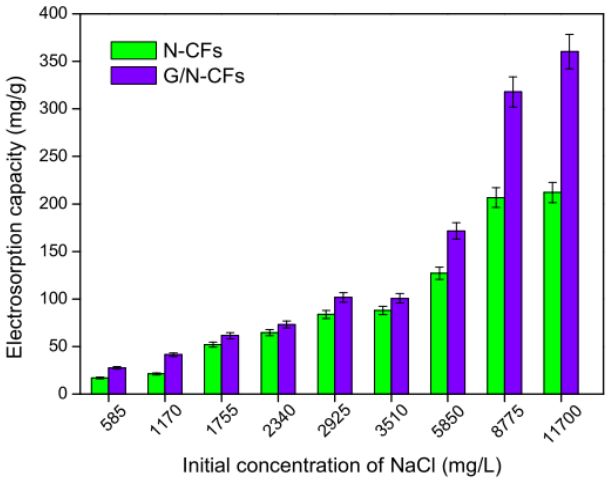

Fig. 7. Electrosorption capacity of the N-CFs and G/N-CFs electrodes at different NaCl concentrations.

3.4. Additional remarks

It is worthwhile noticing that the N-CFs electrode, whose specific capacitance at 5 mV/s (105.50 F/g) is comparable to that reported by Xu et al [6] for graphene (108.83 F/g), at an initial concentration of 585 mg/L, exhibits an electro-sorption capacity (17.0 mg/g) that largely exceeds that of graphene (4.5 mg/g at an initial concentration of 500 mg/L [6]). Since the N-CFs exhibit an excellent performance despite the greatly smaller SSA (~20 against ~151 m^2/g of graphene [6], respectively), it is argued that nitrogen doping plays a crucial role.

N-doping of the carbon lattice can take place at different stages of the material production process [48], during synthesis (e.g. by the use of a N-containing precursor, as in the present case) or post synthesis (e.g. by conditioning of the produced material through the exposure to a N-containing atmosphere). However, regardless of the doping process details, it is commonly recognised [3,6,16−18,48−51] that besides improving the electrical conductivity, the introduction of hydrophilic functional groups on the electrode surface improves its wettability at the interface with the electrolyte, maximising the surface area utilisation [48] and facilitating the ion diffusion [6]. In particular, Zhao et al. [49] demonstrated that, thanks to the introduction of polar C–N bonds, N-doping dramatically improves the wettability of hierarchical carbon nanocages, featured by a multi-scale porous structure, similarly to the present fibres. The results of contact angle measurements proved that undoped nanocages are very hydrophobic (the initial contact angle of 126.6° remains almost unchanged for 30 s or longer). In contrast, doped nanocages with 7.9 at% N are very hydrophilic (the initial contact angle is 48.3° and the droplet is completely absorbed within 20 s) [49]. Li et al. [51] produced hydrophilic PAN-based electro-spun carbon nanofibres (to be employed as filler for reinforcement purposes) via a chemical approach using ethylenediamine (EDA) and graphene (Gr). The notable hydrophilicity of the electro-spun PAN-EDA-Gr fibres (measured contact angle approaching 0° [51]) was ascribed to the N-doping during the high-temperature (850°C) carbonisation with the EDA acting as N source, which changed the wettability of the final product [51].

Our conclusion that the wettability associated to the high level of N-doping of the fibres plays a key role in determining their outstanding electro-sorption capacity further agrees with the picture drawn by Xu et al [16] on N-doped graphene. According to the scheme of the electrochemical reaction process proposed for N-doped graphene in NaCl solution (Fig. S8), the presence of electrochemically active (pyridinic and pyrrolic) N atoms results in

plentiful Na^+ ions accumulated on the electrode surface. In turn, the larger number of H_2O molecules around the Na^+ ions may favour the occurrence of an oxidation/reduction reaction between H_2O and pyridinic or pyrrolic nitrogen [16,52]

$$-\underset{H}{C}=NH + 2e^- + H_2O \leftrightarrows -CH-NHOH$$

As a result, the wettability of the electrode interface is improved, which is beneficial to enlarging the available surface area [48] and improving the charge storage, as recognised also by other research groups [17].

Indeed, a correlation seems to exist between SSA and N-content of the nanocarbons, as determined by the carbonisation temperature (Fig. S9). Carbons carbonised at higher temperature are endowed with very large SSA, but the higher the SSA, the smaller the N-content, and, as a result, the higher their hydrophobicity. The high surface tension caused by hydrophobicity generates “dead pores” as it makes micropores not to be entirely accessible [18]. On the contrary, the highly hydrophilic nature of the electrode surface deriving from the very high levels of N doping renders the micropores entirely accessible. In the case of G/N-CFs, this allows fully profiting of the presence of a large fraction of mesopores and macropores (inset of (Fig. 2b), with graphene-enrichment affording for higher conductivity and capacitance, so as G/N-CFs finally provide an even better performance in CDI of water. At an initial concentration of 585 mg/L, G/N-CFs are able to remove 27.6 mg/g of salt from the NaCl solution, a superior quantity with respect to that electro-sorbed, at the same voltage, by N-doped graphene sponge (21.0 mg/g at an initial concentration of 500 mg/L [6]). Therefore, at the best of the authors’ knowledge, G/N-CFs outperform all the other carbonaceous CDI electrode materials. At the same voltage, a comparable electro-sorption capacity (24.2 mg/g) has been reported for hybrid graphene aerogel/anatase (GA/TiO_2) composites only at an initial concentration (6000 mg/L) higher by more than a factor of 10 [4].

4. Conclusion

Electro-spinning followed by carbonisation at low temperature (500°C) is demonstrated to be an extremely simple method to synthesise highly nitrogen doped carbon fibres to be used as electrode materials for the electrochemical desalination of water with no need of any activation pre-treatment. The low carbonisation temperature, resulting in lower energy consumption and limited release of volatile N-containing by-products, makes the fibre production process cheaper and safer.

The nitrogen doping dramatically improves the wettability of the electrode surface resulting in remarkable electro-sorption capacity (17.0 mg/g at an initial NaCl concentration of 585 mg/L) despite the moderate specific surface area (~20 m^2/g) of the electrode. This opens the way to the realisation of highly performing CDI electrode materials without using harsh chemical oxidants with beneficial effects on the environmental impact of the process.

Unprecedented electro-sorption capacities (27.6 mg/g at an initial NaCl concentration of 585 mg/L) are obtained thanks to the fibre enrichment with graphene, which improves their conductivity and capacitance, while the nitrogen-doping induced higher wettability allows fully profiting of the more favourable pore size distribution in the hybrid fibres.

Acknowledgements

The research leading to CDI results has received funding from the European Union’s H2020 research and innovation programme under grant agreement No. 696656 Graphene Flagship_GrapheneCore1.

References

[1] Y. Oren, Capacitive deionization (CDI) for desalination and water treatment — past, present and future (a review), Desalination 22 (2008) 10−29.

[2] S. Porada, R. Zhao, A. van der Wal, V. Presser, P.M. Biesheuvel, Review on the science and technology of water desalination by capacitive deionization, Progr. Mater. Sci. 58 (2013) 1388–1442.

[3] Z. Wang, T. Yan, J. Fang, L. Shi, D. Zhang, Nitrogen-doped porous carbon derived from a bimetallic metal – organic framework as highly efficient electrodes for flow-through deionization capacitors, J. Mater. Chem. A 4 (2016) 10858–10868.

[4] H. Yin, S. Zhao, J. Wan, H. Tang, L. Chang, L. He, H. Zhao, Y. Gao, Z. Tang, Three-Dimensional Graphene/Metal Oxide Nanoparticle Hybrids for High-Performance Capacitive Deionization of Saline Water, Adv. Mater. 25 (2013) 6270–6276.

[5] P. M. Biesheuvel, Thermodynamic cycle analysis for capacitive deionization, J. Colloid Interface Sci. 332 (2009) 258−264.

[6] X. Xu, Z. Sun, D.H.C. Chua, L. Pan, Novel nitrogen doped graphene sponge with ultrahigh capacitive deionization performance, Sci. Rep. 5 (2015) 11225 (9pp).

[7] N. Zhu, W. Liu, M. Xue, Z. Xie, D. Zhao, M. Zhang, J. Chen, T. Cao, Graphene as a conductive additive to enhance the high-rate capabilities of electrospun $Li_4Ti_5O_{12}$ for lithium-ion batteries, Electrochimica Acta 55 (2010) 5813–5818.

[8] M. Zhang, F. Yan, X. Tang, Q. Li, T. Wang, G. Cao, Flexible CoO – graphene – carbon nano fi ber mats as binder-free anodes for lithium-ion batteries with superior rate capacity and cyclic stability, J. Mater. Chem. A 2 (2014) 5890−5897.

[9] H. Liu, Y. Zhang, R. Li, X. Sun, S. Désilets, H. Abou-Rachid, M. Jaidann, L.S. Lussier, Structural and morphological control of aligned nitrogen-doped carbon nanotubes, Carbon 48 (2010) 1498–1570.

[10] Y. Shao, S. Zhang, M.H. Engelhard, G. Li, G. Shao, Y. Wang, J. Liu, I.A. Aksay, Y. Lin, Nitrogen-doped graphene and its electrochemical applications, J. Mater. Chem. 20 (2010) 7491–7496.

[11] Y. Qiua, J. Yu, T. Shi, X. Zhou, X. Bai, J.Y. Huanga, Nitrogen-doped ultrathin carbon nanofibers derived from electrospinning: Large-scale production, unique structure, and application as electrocatalysts for oxygen reduction, J. Power Sou. 196 (2011) 9862–9867.

[12] L. Qie, W.M. Chen, Z.H. Wang, Q.G. Shao, X. Li, L.X. Yuan, X.L. Hu, W.X. Zhang, Y.H. Huang, Nitrogen-Doped Porous Carbon Nanofiber Webs as Anodes for Lithium Ion Batteries with a Superhigh Capacity and Rate Capability, Adv. Mater. 24 (2012) 2047–2050.

[13] G.S. Park, J.S. Lee, , S.T. Kim, S. Park, J. Cho, Porous nitrogen doped carbon fiber with churros morphology derived from electrospun bicomponent polymer as highly efficient electrocatalyst for Zneair batteries, J. Power Sou. 243 (2013) 267–273.

[14] J. Hou, C. Cao, F. Idrees, X. Ma, Hierarchical Porous Nitrogen-Doped Carbon Nanosheets Derived from Silk for Ultrahigh-Capacity Battery Anodes and Supercapacitors, ACS Nano 9 (2015) 2556–2564.

[15] M.K. Dufficy, S.A. Khan, nd P.S. Fedkiw, Hierarchical Graphene-Containing Carbon Nano fibers for Lithium-Ion Battery Anodes, ACS Appl. Mater. Interfaces 8 (2016) 1327−1336.

[16] X. Xu, L. Pan, Y. Liu, T. Lu, Z. Sun, Enhanced capacitive deionization performance of graphene by nitrogen doping, J. Colloid .Interf. Sci. 445 (2015) 143–150.

[17] K. Shi, M. Ren, I. Zhitomirsky, Activated Carbon-Coated Carbon Nanotubes for Energy Storage in Supercapacitors and Capacitive Water Purification, ACS Sustainable Chem. Eng. 2 (2014) 1289−1298.

[18] Y. Li, J. Shen, J. Li, X. Sun, J. Shen, W. Han,L. Wang, A protic salt-derived porous carbon for efficient capacitive deionization: Balance between porous structure and chemical composition, Carbon 116 (2017) 21–32.

[19] C. Kim, B.T.N. Ngoc, K.S. Yang, M. Kojima, Y.A. Kim, Y.J. Kim, M. Endo, S.C. Yang, Self-Sustained Thin Webs Consisting of Porous Carbon Nanofibers for Supercapacitors via the Electrospinning of Polyacrylonitrile Solutions Containing Zinc Chloride, Adv. Mater. 19 (2007) 2341–2346

[20] C. Kim, Y. Il Jeong, B.T.N. Ngoc, K.S. Yang, M. Kojima, Y.A. Kim, M. Endo, J.W. Lee, Synthesis and Characterization of Porous Carbon Nanofibers with Hollow Cores Through the Thermal Treatment of Electrospun Copolymeric Nanofiber Webs, Small 3 (2007) 91–95

[21] G. Faggio, V. Modafferi, G. Panzera, D. Alfieri, S. Santangelo, Micro-Raman and photoluminescence analysis of composite vanadium oxide/poly-vinyl acetate fibres synthesized by electrospinning, J. Raman Spectr. 43 (2012) 761–768

[22] F. Pantò, Y. Fan, P. Frontera, S. Stelitano, E. Fazio, S. Patanè, M. Marelli, P.L. Antonucci, F. Neri, N. Pinna, S. Santangelo, Are electrospun carbon/metal oxide composite fibres relevant electrode materials for Li-ion batteries?, J. Electrochem. Soc. 163 (2016) A2930-A2937

[23] M.S.A. Rahaman, A.F. Ismail, A. Mustafa, A review of heat treatment on polyacrylonitrile fiber, Polymer Degradation and Stability 92 (2007) 1421–1432

[24] W. S. Hummers, R. E. Offeman, Preparation of graphitic oxide, *J. Am. Chem. Soc.* **1958**, *80*, 1339–1339.

[25] R. Zhang, S. Santangelo, E. Fazio, F. Neri, M. D'Arienzo, F. Morazzoni, Y. Zhang, N. Pinna, P.A. Russo, Stabilization of TiO_2 nanoparticles at the surface of carbon nanomaterials promoted by microwave heating, *Chemistry – A European Journal* 21 (2015) 14901–14910

[26] J.I. Paredes, S. Villar-Rodil, A. Martínez-Alonso, J. M. D. Tascón, Graphene Oxide Dispersions in Organic Solvents, Langmuir 2008, 24, 10560 – 10564

[27] M. Bognitzki, W. Czado, T. Frese, A. Schaper, M. Hellwig, M. Steinhart, A. Greiner, J.H. Wendorff, Nanostructured Fibers via Electrospinning, *Adv. Mater.* 13 (2001) 70–72

[28] Z. Zhou, C. Lai, L. Zhang, Y. Qian, H. Hou, D.H. Reneker, H. Fong, Development of carbon nanofibers from aligned electrospun polyacrylonitrile nanofiber bundles and characterization of their microstructural, electrical, and mechanical properties, Polymer 50 (2009) 2999–3006

[29] X. Liu, J. Zhang, S. Guo, N. Pinna, Graphene/N-doped carbon sandwiched nanosheets with ultrahigh nitrogen doping for boosting lithium-ion batteries, *Journal of Materials Chemistry A* 4 (2016) 1423-1431.

[30] H. Zhang, P. Liang, Y. Bian, Y. Jiang, X. Sun, C. Zhang, X. Huang, F. Wei,Moderately oxidized graphene – carbon nanotubes hybrid for high performance capacitive deionization, RSC Adv. , 2016, 6 , 58907–58915

[31] T.F. Baumann, M.A. Worsley, T.Y.J. Han, J.H. Satcher Jr., High surface area carbon aerogel monoliths with hierarchical porosity, J. Non-Crystalline Solids 354 (2008) 3513–3515

[32] M. E. Suss, T. F. Baumann, W. L. Bourcier, C. M. Spadaccini, K. A. Rose, J. G. Santiago, M. Stadermann, Capacitive desalination with flow-through electrodes, Energy&Environmental Science 5 (2012) 9511-9519

[33] M.E. Suss, S. Porada, X. Sun, P.M. Biesheuvel, J. Yoon, V. Presser, Water desalination via capacitive deionization: what is it and what can we expect from it?, Energy & Environmental Science 2015, 8, 2296-2319.

[34] F. Rouquerol, J. Rouquerol, K.S.W. Sing, P. Llewellyn, G. Maurin, Adsorption by powerds and porous solids. Principles, methodology and applications, Ed. Elseiver Ltd., IBSN 978-0-08-097035-6, 2014.

[35] M. Thommes, Physical Adsorption Characterization of Nanoporous Materials, Chem. Ing. Tech. 82 (2010) 1059-1073. Doi:10.1002/cite.201000064.

[36] S. Liu, C. Deng, L. Yao, H. Zhong, H. Zhang, The key role of metal dopants in nitrogen-doped carbon xerogel for oxygen reduction reaction, J. Power Sou. 269 (2014) 225-235.

[37] Y. Wang, S. Serrano, J.J. Santiago-Avilés, Raman characterization of carbon nanofibers prepared using electrospinning, Synthetic Metals 138 (2003) 423–427.

[38] A. C. Ferrari, J. Robertson, Interpretation of Raman spectra of disordered and amorphous carbon, Phys. Rev. B 61 (2001) 14095–14107.

[39] S. Santangelo, Controlled surface functionalization of carbon nanotubes by nitric acid vapors generated from sub-azeotropic solution. Surf Interface Anal 2016;48:17−25.

[40] F. Tuinstra, J.L. Koening, Raman spectrum of graphite, J. Chem. Phys. 53 (1970) 1126–1130.

[41] M.B. Vázquez-Santos, E. Geissler, K. László, J.N. Rouzaud, A. Martínez-Alonso, J.M.D. Tascón, Comparative XRD, Raman, and TEM Study on Graphitization of PBO-Derived Carbon Fibers, J. Phys. Chem. C 116 (2012) 257–268.

[42] W. Shi, H. Li, X. Cao, Z.Y. Leong, J. Zhang, T. Chen, H. Zhang, H.Y. Yang, Ultrahigh performance of novel capacitive deionization electrodes based on a three-dimensional graphene architecture with nanopores, Sci. Rep. 6 (2015) 18996 (9pp).

[43] M. Noked, E. Avraham, A. Soffer, D. Aurbach, The rate-determining step of electroadsorption processes into nanoporous carbon electrodes related to water desalination, *J. Phys. Chem. C*, 113 (2009) 21319−21327.

[44] H. Li, Y. Gao, L. Pan, Y. Zhang, Y. Chen, Z. Sun, Electrosorptive desalination by carbon nanotubes and nanofibres electrodes and ion-exchange membranes, Water Res. 42 (2008) 4923–4928.

[45] R. Zhao, P.M. Biesheuvel, H. Miedema, H. Bruning, A. Van der Wal, Charge efficiency: a functional tool to probe the double –layer structure inside of porous electrodes and application in the modeling of capacitive deionization, J. Phys. Chem. Lett. 1 (2010) 205–210.

[46] H Li, L. Pan, T. Lu, Y. Zhan, C. Nie, Z. Sun, A comparative study on electrosorptive behaviour of carbon nanotubes and graphene for capacitive deionization, Journal of Electrochemical chemistry 653 (2011) 40–44.

[47] T. Zhang, H. Zhao, X.X. Huang, G. Wen, Li-ion doped graphene/carbon nanofiber porous architectures for electrochemical capacitive desalination, Desalination 379 (2016) 118–125.

[48] L. Chen, T. Ji, L. Mu, J. Zhu, Cotton fabric derived hierarchically porous carbon and nitrogen doping for sustainable capacitor electrode, Carbon 111 (2017) 839–848.

[49] J. Zhao, H. Lai, Z. Lyu, Y. Jiang, K. Xie, X. Wang, Q. Wu, L. Yang, Z. Jin, Y. Ma, J. Liu, Z. Hu, Hydrophilic hierarchical nitrogen-doped carbon nanocages for ultrahigh supercapacitive performance, Adv. Mater. 27 (2015) 3541–3545.

[50] K.V. Kumar, K. Preuss, Z.X. Guo, M.M. Titirici, Understanding the hydrophilicity and water adsorption behavior of nanoporous nitrogen-doped carbons, J. Phys. Chem. C 120 (2016) 18167–4818179.

[51] Z. Li, O. Zabihi, J. Wang, Q. Li, J. Wang, W. Lei, M. Naebe, Hydrophilic PAN based carbon nano fi bres with improved graphitic structure and enhanced mechanical performance using ethylenediamine functionalized graphene, RSC Adv. 7 (2017) 2621–2628.

[52] L. Sun, L. Wang, C. Tian, T. Tan, Y. Xie, K. Shi, M. Li, H. Fu,Nitrogen-doped graphene with high nitrogen level via a one-step hydrothermal reaction of graphene oxide with urea for superior capacitive energy storage, RSC Advances 2 (2012) 4498–4506.

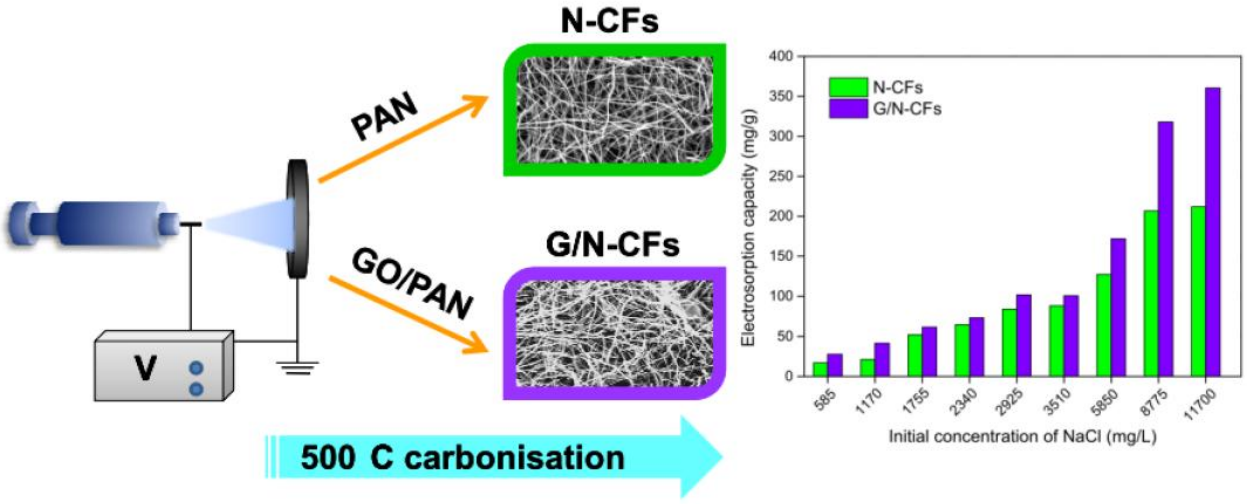

Graphical abstract

Highlights

► Pure and graphene-enriched C fibres with high N contents (19−21 wt%) are prepared by electro-spinning

► The fibres are tested as electrodes for capacitive deionization of water without any pre-treatment

► The fibrous electrodes remove 17.0−27.6 mg/g of NaCl from a solution with a 585 mg/L initial concentration

► Graphene-enrichment improves conductive and electro-sorptive properties of the fibres

► The high fibre wettability due to the large N contents is responsible for the huge electro-sorption capacity